Multilayered Nano-Architecture of Variable Sized Graphene Nanosheets for Enhanced Supercapacitor Electrode Performance

Sanjib Biswas and Lawrence T. Drzal*

Department of Chemical Engineering and Materials Science and Composite Materials and Structures Center, Michigan State University, East Lansing, Michigan 48824-1226

ABSTRACT The diverse physical and chemical aspects of graphene nanosheets such as particle size surface area and edge chemistry were combined to fabricate a new supercapacitor electrode architecture consisting of a highly aligned network of large-sized nanosheets as a series of current collectors within a multilayer configuration of bulk electrode. Capillary driven self-assembly of monolayers of graphene nanosheets was employed to create a flexible, multilayer, free-standing film of highly hydrophobic nanosheets over large macroscopic areas. This nanoarchitecture exhibits a high-frequency capacitative response and a nearly rectangular cyclic voltammogram at 1000 mV/s scanning rate and possesses a rapid current response, small equivalent series resistance (ESR), and fast ionic diffusion for high-power electrical double-layer capacitor (EDLC) application.

KEYWORDS: highly aromatic graphene • electronic properties • electrochemical capacitors • binder-free electrode • multilayer free-standing film • aligned nanostructure

INTRODUCTION

Graphene, a two-dimensional aromatic macromolecule, is the basic building block for different allotropes of carbon such as carbon nanotubes (CNT), fullerene, and graphite (1−6). Exceptional electrical, thermal, and mechanical properties along with facile manufacturing techniques make this inexpensive, two-dimensional monolayer allotrope of carbon unique from other graphitic dimensionalities (1−6). Acid intercalation followed by thermal exfoliation of natural graphite is an easy approach to produce exfoliated graphene nanosheets with a surface area about 270 m^2/g and an average thickness of 3−5 nm with a lateral dimension ranging from sub micrometer to more than 50 μm (7). These nanosheets with stacks of few single-layer graphene preserve the aromaticity without requiring any extensive chemical oxidation treatment of the graphene basal plane to exhibit low electrical resistivity of 50×10^{-6} ohm cm (7). Retention of aromaticity of graphene and the absence of significant oxygen functionalities on the graphene basal plane result in high thermal stability (2 wt % loss in air) of these nanosheets in the temperature range from 120 to 350 °C, where a considerable weight loss is expected for highly oxidized graphene basal plane from the generation of decomposed gaseous products such as CO and CO_2 (8−10) (see the Supporting Information). XPS elemental analysis further confirms the high degree of aromaticity with a C/O atomic ratio close to 25.7 (see the Supporting Information). However, the high degree of hydrophobicity, resulting from the aromaticity, prohibits the dispersion of these nanosheets in water and other polar liquids and results in agglomeration even after extended sonication (11, 12). The key to the success of exploiting the unique properties of graphene nanosheets lies in the homogeneous and orderly distribution of these nanosheets from the nanoscale to the macroscale regime. The primary challenge is to overcome the self-aggregation following the strong van der Waals force of attraction between the large and planar basal planes. Liquid−liquid interfacial adsorption is one approach to overcome this self-aggregation to create a monolayer film of these hydrophobic nanosheets from the minimization of interfacial energy at the hydrophobic liquid-hydrophilic liquid interface (12).

An aligned network of these highly electrically conductive graphene nanosheets is expected to demonstrate reduced electronic resistance and rapid charge discharge characteristics for electrochemical energy storage applications. Capillary-force-driven self-assembly of vertically aligned carbon nanotubes into a highly dense and compact structure for electrochemical energy storage application such as electrical double layer capacitors (EDLC) has been well-documented in different publicaiotns (13−15). However, the construction of an aligned network of CNT from a previously grown bulk carbon nanotube forest on a large macroscopic area often results in formation of microcracks or open cellular structure during the collapse and shrinkage of the CNTs by the capillary force and drying induced condensation (16−18). This kind of microcrack formation is universal during the drying induced shrinkage of bulk materials such as mud, clay, and others. Instead of using bulk material in an analogous capillary force driven self-assembly process we introduce a "bottom-up" approach, starting with a monolayer film of graphene nanosheets to create a highly aligned
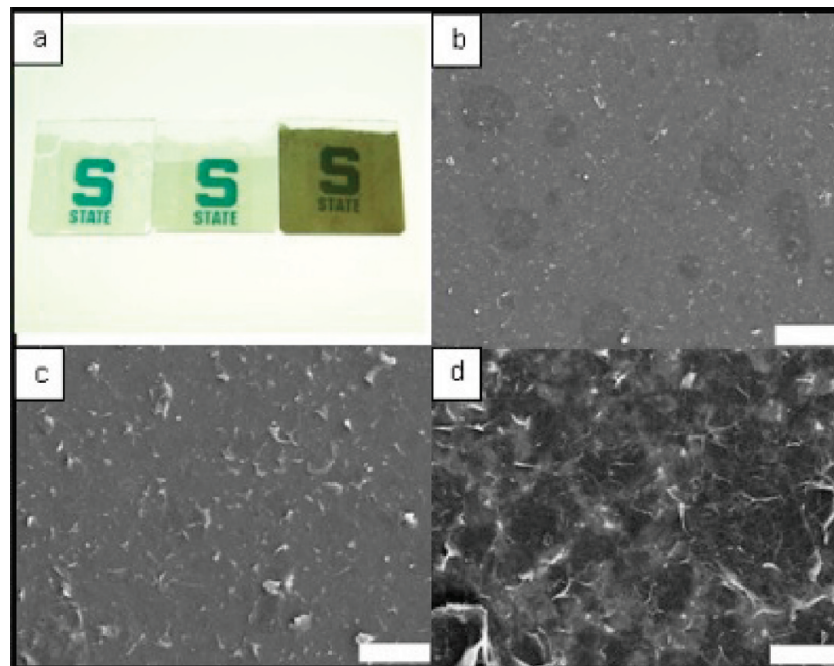
FIGURE 1. Multilayer structure of graphene nanosheets from successive depositions of monolayer films one on top of another. (a) Stable monolayer, bilayer, and multilayer (four layers) films were deposited on glass substrate (scale bar 1 cm). Under the marked arrow in the middle slide, two monolayer films were deposited one on top of another to create a stable bilayer structure. The optical transparency also decreases linearly with increasing number of depositing layers. (b−d) From the FESEM morphological characterization beginning with image b, a substantial overlap between nanosheets was observed from the monolayer to multilayer configuration in image d (scale bars 50, 20, and 10 μm, respectively).

multilayer, free-standing film over large macroscopic areas. The capacitive response of this aligned multilayer configuration is explored for rapid charge discharge characteristics in high power EDLC applications. The impact of physical and chemical aspects of the graphene nanosheets such as particle size, alignment, and surface chemistry is investigated in optimizing the performance of graphene nanosheets based electrodes for EDLC applications.

RESULT AND DISCUSSION

In the liquid−liquid interfacial adsorption technique, nanosheets of average lateral dimension of 15 μm and thickness of 3−5 nm were first dispersed in chloroform followed by the addition of a small amount of water to create a two-phase mixture. This two-phase mixture was then briefly sonicated to create a large interfacial area between the two immiscible liquids. At this point, the transport of graphene nanosheet from the bulk phase toward the liquid−liquid interface was driven by the minimization of interfacial energy (12). The interfacial self-assembly approach has the advantage to create a highly dispersed monolayer network of hydrophobic nanosheets over a large macroscopic area without requiring any chemical transformation of the graphene basal plane (12). With the retention of this strong aromatic character, layers of these highly dispersed networks of graphene nanosheets were expected to interact strongly with each other in a "face-to-face" union of large basal planes. van der Waals force induced stacking of these nanosheets is the key to our approach to create a highly aligned, multilayer structure from successive depositions of close packed monolayer films one on top of another.

In creating a multilayer structure, first a monolayer film of graphene nanosheets was transferred to a solid substrate such as a microscopic glass slide (Figure 1a). The film was then annealed at 100 °C to completely drive off the liquid. When a second layer of monolayer film was transferred on top of the first one, a thin film of water always separates these nanosheets preventing close contact with each other. With continuous evaporation of water, the interlayer separation decreases and the strong capillary force causes the nanosheets spacing to decrease and the layers to collapse on each other. On complete liquid evaporation, strong van der Waals forces of attraction adhere these planar nanosheets into a stable bilayer structure. The bilayer film was annealed again at 100 °C (Figure 1a, middle slide).

As compared to spherical points or parallel chain molecules, the van der Waals interaction free energy between two parallel planes is much higher and it scales with the separation distance (d) as ($1/d^2$) (19, 20). Thus when two monolayer films of planar nanosheets are placed one on top of another, a large van der Waals force of attraction causes them to adhere with each other and form a stable bilayer and multilayer structure. It is also possible that the π-electron interaction between the large basal planes contributes to this interaction (19, 20).

This process of capillary- and drying-induced self-assembly of successive monolayers is continued to build a multilayer film of desired thicknesses. The film can then be detached from the solid substrate by immersing it in water, which slowly wets the glass surface and causes the displacement of this highly hydrophobic film from the glass surface
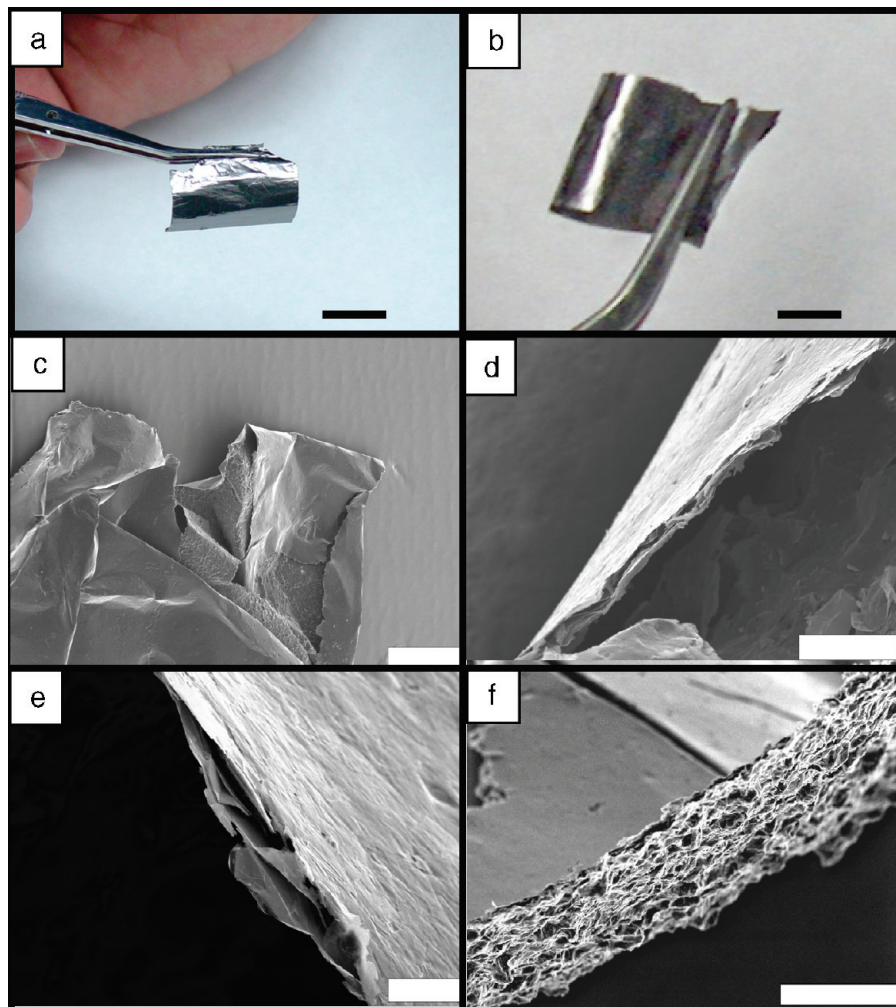
FIGURE 2. Characterization of the morphology of the multilayer, free-standing film. (a, b) Film is flexible and can be bent or rolled (scale bar 1 cm). (c) FESEM micrograph clearly shows a crumpled film without the formation of large fragments or cracks (scale bar 500 μm). (d–f) Films of various thicknesses from less than 5 μm to more than 50 μm (scale bar 20, 5, and 200 μm respectively).

to a state where it floats on the water surface (see the Supporting Information). The film is then dried at 100 °C to obtain a free-standing, multilayer film of graphene nanosheets as shown in Figure 2. FESEM micrographs clearly show that the film is flexible without any cracks over the large macroscopic area.

As shown in Figure 2d–f, films of various thicknesses can be prepared by controlling the number of deposited layers. This process results in the formation of a 100% binder free multilayer, free-standing film of graphene nanosheets uniformly dispersed and strongly attached to each other over a large macroscopic area. The graphene nanosheets comprising this film are highly aromatic in character and the interlayer attraction between the large basal planes is dominated by van der Waals force rather than the interlayer hydrogen bonding reported for chemically modified graphite oxide basal planes (8, 9). TGA analysis showed no appreciable weight loss (<4 wt % in air) in the temperature range between 100 to 350 °C, where a considerable weight loss was reported for graphite oxide based systems owing to the release of interlayer water molecules and the decomposition of the surface oxides resulting in a mixture of CO and CO_2 from the various oxygen functionalities present on

the graphene basal plane (8–10) (see the Supporting Information). The highly hydrophobic character of the film was also evident from the large contact angle (~96.7°) formed by a water droplet on the film (see the Supporting Information). With the absence of interlayer hydrogen bonding and the presence of turbostratic stacking of graphene nanosheets in different layers, the film is strong enough to hold together over large macroscopic areas even when completely bent and rolled into a cylindrical shape (see the Supporting Information). The Raman spectra, measured on the multilayer film, exhibits a sharp G band peak at 1575 cm^{-1} and a minor D band peak at 1344 cm^{-1} (see the Supporting Information). The aromatic purity of the film is also evident from this low $I(D)/I(G)$ ratio, which is a direct measure of the degree of defects, disorder, and structural incoherence of crystalline graphitic domain of the large basal plane on graphene nanosheets (21–23). As a result the "as-prepared" multilayer film exhibits very high electrical conductivity of the order of 1.24×10^4 S/m, measured by using a four-point probe set up on an average of four samples.

Self-assembly of these successive monolayers can also be accomplished on metal substrates such as a stainless steel substrate to create a multilayer configuration of graphene
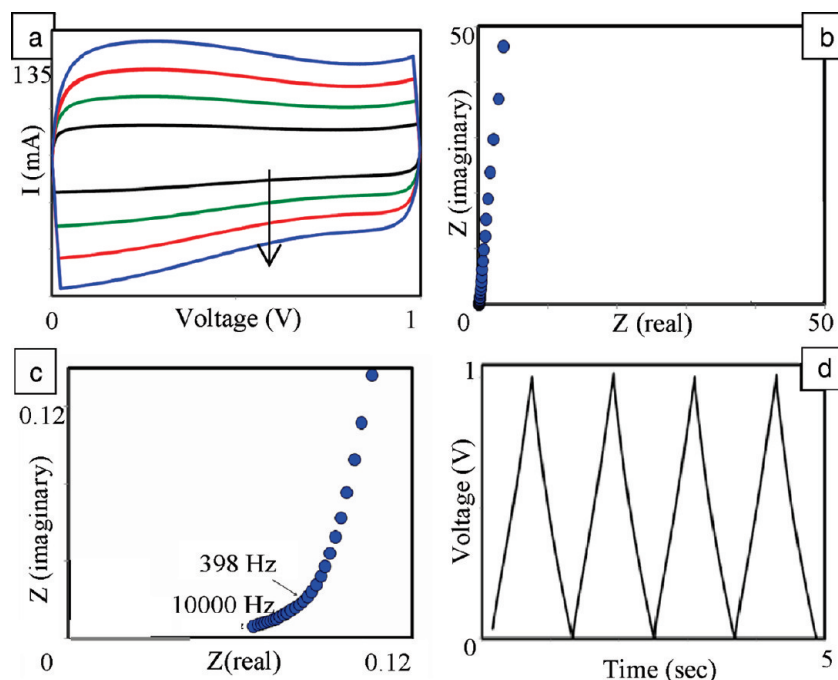
FIGURE 3. Electrochemical characteristics of multilayer graphene nanosheet film. (a) Retention of nearly rectangular CV at high scanning rates from 250 to 1000 mV/s. (b) Complex plane impedance analysis from high to low frequency. (c) Impedance analysis at high-frequency region with the knee frequency appearing close to 398 Hz. (d) Highly symmetric charge–discharge characteristics at current density 30 A/g.

nanosheets as a 100% binder-free electrode for EDLC application (see the Supporting Information). For this purpose, thin film electrodes with an average thickness of 20 μm were assembled in a two-electrode configuration and the assembly was immersed in aqueous 6 M KOH solution for electrochemical measurements. In EDLC applications, a highly oblique and narrow shaped capacitance–voltage response at high scanning rate is highly undesirable (24). This shape results from large internal and interfacial contact resistance of the active material inside the bulk electrode (24). From Figure 3a, a nearly rectangular and highly symmetric cyclic voltammogram (CV) curve at an increasing voltage scanning rate from 250 to 1000 mV/s clearly demonstrates rapid current response, small equivalent series resistance (ESR) and fast ionic diffusion within the aligned network of graphene nanosheets for this multilayer film electrode. Retention of aromaticity of the graphene basal plane and the strong overlap between these large-sized nanosheets from different layers create a highly conducting network with minimum internal resistance over the macroscopic area of the film. In comparison to other allotropes of carbon, these two-dimensional nanosheets lay flat on the solid substrate to generate a large contact area between the active electrode material and the current collector surface.

The impact of low internal resistance and minimum interfacial contact resistance with the current collector was evident from the high frequency capacitative response of the electrode with a knee frequency close to 398 Hz, as shown in Figure 3b, c. The appearance of high knee frequency was only comparable to the performance of highly aligned carbon nanotube network directly grown on the current collector surface (25–27). From the Bode plot, a phase angle close to 90° up to a frequency of 10 Hz clearly suggests the

device functionality close to an ideal capacitor (see the Supporting Information). The average specific capacitance, measured from the discharge slope (shown in Figure 3d) at constant current density 30 A/g was close to 36 F/g, which is comparable to the capacitance obtained with highly aligned carbon nanotube electrodes (25–27).

To investigate the role of edge functionalities and the impact of particle dimension of graphene nanosheets on the capacitative response and the bulk resistivity of the electrode, we prepared small-sized nanosheets with an average dimension of 500 nm by mechanical milling of large-sized nanosheets without applying any oxidative chemical cleavage of large basal planes (7). The increase in the surface area of the small-sized nanosheets to 550 m^2/g is concomitant with a proportional increase in the ratio of the edge to basal plane area on going from large to small sized nanosheets. XPS analysis of these small sized nanosheets also exhibits an increase in the oxygen atomic concentration to 6.5 from 3.7% for the large-sized nanosheets (see the Supporting Information). Thus with increasing edge to basal plane area, the relative proportion of oxygen functional groups bound to the active edge sites of these nanosheets increases. Although the presence of these oxygen functionalities enhances the wettability of the electrode, the decreasing particle size on the other hand significantly contributes toward a larger electronic resistivity of the electrode from increasing inter particle contact resistance. To retain high electronic conductivity of the electrode, here we combine the large- and small-sized nanosheets in an aligned conformation to achieve enhanced capacitance while maintaining facile electronic conduction at minimum loading of large-sized nanosheets inside the bulk electrode.
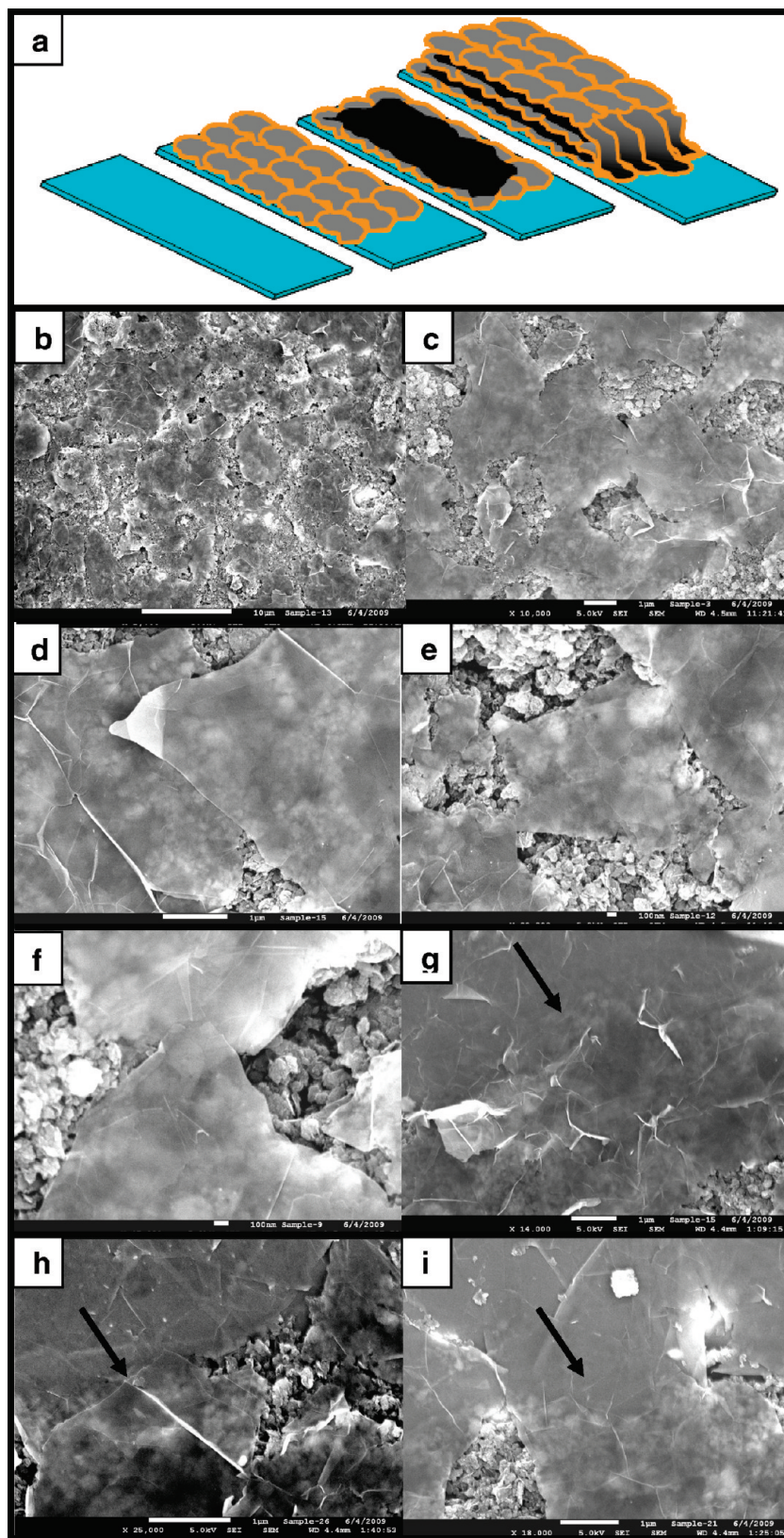
FIGURE 4. Fabrication of aligned composite of large and small sized nanosheets. (a) Representative schematic diagram demonstrating the development of layered structure starting with a stainless steel substrate that was then coated with monolayer of large-sized nanosheets followed by the deposition of layers of small-sized nanosheets. A monolayer of large-sized nanosheets was then deposited on top of the smaller ones, not only covering the small sized nanosheets but also extending to the top section covered by the first monolayer film of large nanosheets. This layer-by-layer deposition continues to develop a multilayer structure as shown by the right-most representative schematic image in panel a. (b–f) FESEM characterization clearly showing a monolayer coverage of large-sized nanosheet placed on top of smaller ones where the large ones are individually connected with each other near their edges. (g–i) Large-sized nanosheets connecting the bulk electrode to the top section where it is attached on the current collector surface; the FESEM micrograph clearly shows how a part of the large-sized nanosheet covers the small-sized ones and then extends to strongly attach itself with other large-sized nanosheets at the top section.
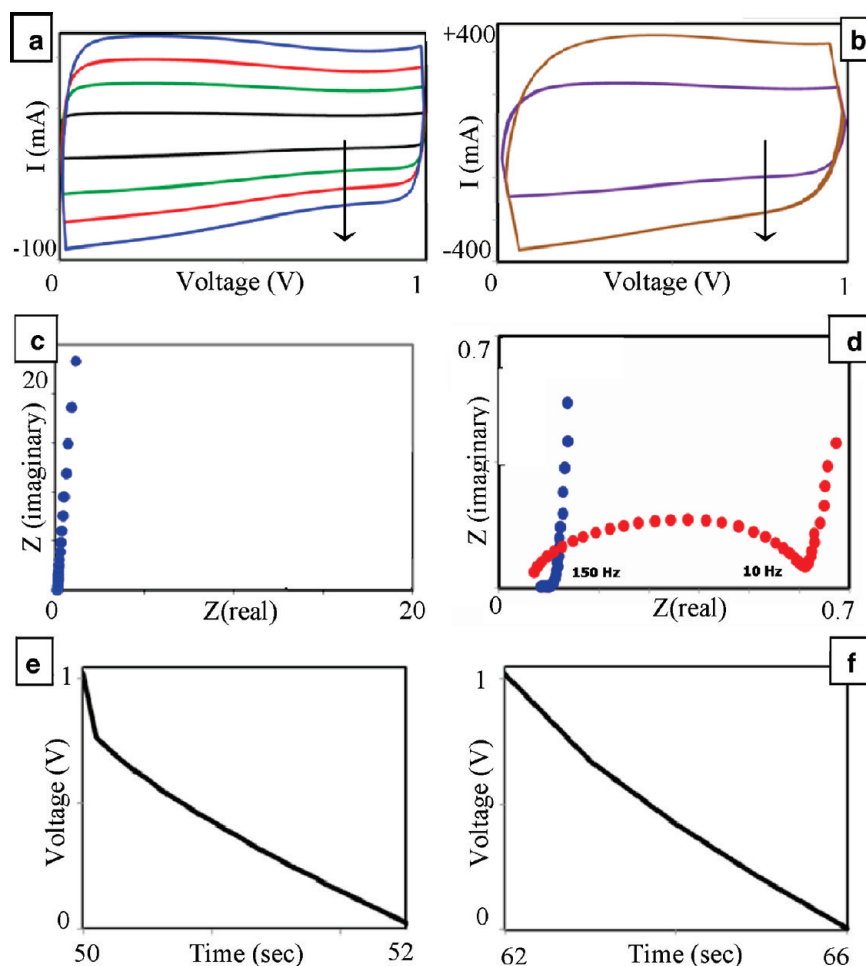
FIGURE 5. Electrochemical characteristics of aligned and randomly mixed composite electrode. (a, b) Nearly rectangular CV of aligned configuration of large- and small-sized nanosheets at increasing voltage scanning rate from 20 to 500 mV/s. (c) Impedance spectra of aligned composite from high to low frequency. (d) High-frequency impedance spectra of aligned and randomly mixed composite with the knee frequency close to 150 and 10 Hz, respectively. (e, f) Constant current discharge characteristics of randomly mixed and aligned configuration at 6 and 10 A/g current densities, respectively.

As described earlier, to minimize the interfacial contact resistance between the current collector and the active electrode material, we first deposited a monolayer or bilayer film of large graphene nanosheets on a stainless steel plate. As explained in the schematic diagram of Figure 4a, multiple layers of small-sized nanosheets were then deposited at less than monolayer densities. Subsequently, another monolayer of large-sized nanosheets was carefully placed to uniformly overlay the small sized nanosheets. From the FESEM characterization in Figure 4 b–f, it is evident that a highly dispersed network of large sized nanosheets could uniformly cover the smaller ones. However, the distributed network of these large-sized nanosheets was not as closely packed as was found on a smooth glass surface as a result of the surface roughness inherent in the layers of the of small-sized nanosheets as compared to the film formed on a clean and smooth glass surface. However, as explained in Figure 4 b–f, these large-sized nanosheets are highly dispersed, laying flat and connected to each other near their edges to create a highly conducting aligned network inside the bulk electrode. The large-sized nanosheets interact with the smaller ones through the large basal plane area and at the same time the large graphene nanosheets are also connected with each

other. The top layer is firmly attached to the current collector surface. As explained in Figure 4g–i, FESEM characterization clearly shows how a part of the large-sized nanosheet covers the small-sized ones and then extends to strongly attach itself with other large-sized nanosheets at the top section.

Specimens of this layered structure were prepared by this method to achieve 3–4 mg/cm^2 loading and an average thickness of 65 μm of active material for electrochemical measurements. For comparison, and to demonstrate the effect of dimension and distribution of conductive fillers on the capacitive response of the bulk electrode, one additional set of electrodes with similar area and mass loading was prepared in a conventional way by mixing small-sized nanosheets with highly conductive carbon black in the presence of a binder.

As can be seen from the CV data in Figure 5a,b, the retention of symmetrical CV response with nearly straight rectangular sides for the aligned configuration at scanning rates as high as 500 mV/s clearly indicates a minimum internal resistivity and excellent electrolyte ionic accessibility throughout the porous structure of the layer assembled electrode. From the impedance analysis, the measured electrode resistance R_c of the aligned configuration is only
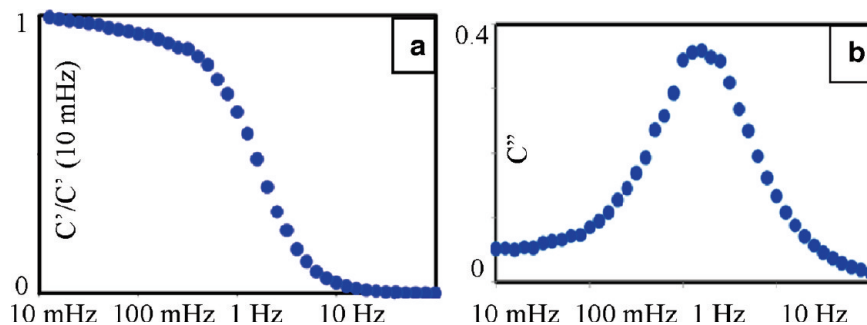
FIGURE 6. Frequency analysis on the real and imaginary part of the capacitance. (a) Variation of the normalized real part of the capacitance $C'(\omega)/C'$ (10 mHz) with decreasing frequency. (b) Determination of relaxation time constant (τ_0) from the imaginary part of the capacitance for the aligned configuration of large- and small-sized nanosheets.

20−30 mohm, which is more than 1 order of magnitude less than electrodes prepared from small-sized nanosheets and carbon black in the conventional way (Figure 5c,d). Moreover, the disappearance of a large semicircle response in the impedance curve at high frequency for the aligned configuration again demonstrates minimum interfacial contact resistance and the uniformity of the coverage of the large-sized nanosheets on the metal current collector surface.

A nearly vertical low-frequency line and a "knee" frequency close to 150 Hz points to the suitability of the aligned configuration for high-power applications as compared to randomly mixed composites where the knee frequency was obtained at around 10 Hz. The high rate capability of the aligned configuration is also evident from the constant current chronopotentiometric measurement. IR drop at the beginning of galvanostatic discharge is an indication of a large internal resistance of the cell (24). As shown in Figure 5e, a significant IR drop for the randomly mixed configurations at a current density of 6 A/g considerably limits its high rate performance as compared to the aligned configuration, which continues to maintain symmetrical charge discharge characteristics even for high discharge current density at 10 A/g. The average specific capacitance of the aligned composite configuration, calculated from the slope of the discharge curve at 10 A/g, was close to 80 F/g. The high electrochemical cyclic stability of this multilayer film electrode was evidenced from the retention of more than 98 % of specific capacitance at the end of 1000 electrochemical cycles.

From the above analysis, we conclude that this aligned configuration utilizing large sized nanosheets not only contributes toward the double layer capacitance but also acts as a series of current collectors within the bulk electrode structure for facile electronic conduction from the internal structure to the current collector surface through the large-sized graphene nanosheets. The high-surface-area, small-sized nanosheets on the other hand enhance the specific capacitance by creating a highly mesoporous network and improving the wettability of the electrodes resulting from the presence of oxygen functional groups present at the edges. Moreover, we have demonstrated that the dimension and distribution of conductive fillers inside the bulk electrode have a major impact on the bulk resistivity toward achieving high-frequency capacitive response for high power applications.

The consequence of particle alignment is further evident from the frequency dependent analysis on the real and imaginary part of the capacitance. A nearly invariant capacitance with decreasing frequency for the aligned configuration makes them ideally suited for supercapacitor applications (28, 29). This is also obvious from the Bode angle plot, with a nearly parallel frequency independent phase angle close to 90° up to a frequency 1 Hz (see the Supporting Information). The determination of the relaxation time constant from the reciprocal of characteristic frequency (f_0) in the frequency-dependent imaginary capacitance analysis quantitatively reveals how fast the capacitor device can be reversibly charged and discharged (28, 29). As shown in Figure 6b, the calculated relaxation time constant for the aligned configuration is only 633 ms, which was found to be more than 1 order of magnitude lower than the randomly mixed counterpart.

CONCLUSION

Self-assembly of graphene nanosheets driven by the minimization of interfacial energy at the liquid−liquid interface has a distinctive advantage for the fabrication of a highly dispersed monolayer network over large macroscopic areas. Previous research employed a vacuum filtration approach from the water or hydrophobic solvent based dispersion of graphite oxide, reduced graphite oxides, and graphene dispersions to produce well packed and highly aligned graphene paper of various thicknesses (8, 9, 30, 31). The use of graphene nanosheets prepared by direct exfoliation as opposed to the graphene oxide route gives rise to a graphene nanosheets without altering the attractive, native chemical properties of graphene basal planes. Retention of the strong aromatic character of the graphene nanosheets prepared in this way causes a large inter planar interaction from the capillary force and drying induced collapse of monolayers of graphene nanosheets into a flexible and 100 % binder-free multilayer, free-standing film. The resulting multilayer film exhibits superior high-frequency capacitive properties with a knee frequency close to 398 Hz and a nearly rectangular cyclic voltammogram at 1000 mV/s for high-power EDLC applications. A major benefit in our approach is that nanomaterials of a desired architecture along with graphene's attractive physical and chemical characteristics can be synthesized into an architecture consisting of large and small graphene

nanosheets into a highly dispersed and aligned network in a bulk macroscopic configuration designed to maximize device performance. Monolayers of large-sized nanosheets function as a series of highly electrically conducting current collectors within the mesoporous network of small-sized graphene nanosheets for improved rate capability of EDLC electrode with a specific capacitance of 80 F/g at a high discharge current density of 10 A/g. These inexpensive graphene nanosheets and the ease of the process to produce the aligned nanostructure make this new material and method highly advantageous for high power supercapacitor applications.

METHODS

Formation of Multilayer Film of Graphene Nanosheets. Nanosheets with an average thickness of 3−5 nm and width 15 μm were first dispersed in chloroform by sonication. In this dispersion, water was added to get a two-phase mixture of water and chloroform. This two-phase mixture was then briefly sonicated to get the nanosheets absorbed at the liquid−liquid interface. Once the nanosheets were adsorbed at the interface, they could not be brought back to the bulk phase even after vigorous shaking. However, upon shaking, at the interface numerous emulsion droplets were formed with the nanosheets still covering the interface between the two immiscible liquids. Droplets, reaching the air−water interface, spread in the form of a thin film and the rapid evaporation of chloroform results in a dry film of graphene nanosheet floating at the air−water interface. This film was then lifted by pulling a substrate through the air−water interface. It was then heated at 100 °C to remove the residual water. Multilayer film was formed by successive depositions of these monolayer films one on top of another.

Detachment of Multilayer Film from the Glass Substrate. For detachment, the multilayer film on the glass substrate was immersed in slightly warm water at around 50−60 °C for a few hours. At this condition, water slowly wets the glass surface and causes the displacement of this highly hydrophobic film from the glass surface to a state where it floats on the water surface. The film was then carefully lifted and dried at 100 °C.

Supporting Information Available: Experimental procedure and extensive figures (PDF). This information is available free of charge via the Internet at http://pubs.acs.org.

REFERENCES AND NOTES

(1) Geim, A. K.; Novoselov, K. S. *Nat. Mater.* **2007**, *6*, 183−191.
(2) Castro, A.H. N.; Guinea, F.; Peres, N. M. R.; Novoselov, K. S.; Geim, A. K. *Rev. Mod. Phys.* **2009**, *81*, 109−162.
(3) Jang, B. Z.; Zhamu, A. *J. Mater. Sci.* **2008**, *43*, 5092−5101.
(4) Avouris, P.; Chen, Z.; Perebeinos, V. *Nat. Nanotechnol.* **2007**, *2*, 605−615.
(5) Rao, C. N. R.; Sood, A. K.; Subrahmanyam, K. S.; Govindaraj, A. *Angew. Chem., Int. Ed.* **2009**, *48*, 7752−7777.
(6) Allen, M. J.; Tung, V. C.; Kaner, R. B. *Chem. Rev.* **2010**, *110*, 132−145.
(7) Drzal, L. T.; Fukushima, H. Expanded graphite and products produced therefrom. U.S. Patent application 20040127621, 2004.
(8) Dikin, D. A.; Stankovich, S.; Zimney, E. J.; Piner, R. D.; Domett, G. H. B.; Evmenenko, G.; Nguyen, S. T.; Ruoff, R. S. *Nature* **2007**, *448*, 457−460.
(9) Park, S.; An, J.; Piner, R. D.; Jung, I.; Yang, D.; Velamakanni, A.; Nguyen, S. T.; Ruoff, R. S. *Chem. Mater.* **2008**, *20*, 6592−6594.
(10) Park, S.; An, J.; Jung, I.; Piner, R. D.; An, S. J.; Li, X.; Velamakanni, A.; Ruoff, R. S. *Nano Lett.* **2009**, *9*, 1593−1597.
(11) Lu, J.; Drzal, L. T.; Worden, R. M.; Lee, I. *Chem. Mater.* **2007**, *19*, 6240−6246.
(12) Biswas, S.; Drzal, L. T. *Nano Lett.* **2009**, *9*, 167−172.
(13) Futaba, D. N.; Hata, K.; Yamada, T.; Hiraoka, T.; Hayamizu, Y.; Kakudate, Y.; Tanaike, O.; Hatori, H.; Yumura, M.; Iijima, S. *Nat. Mater.* **2006**, *5*, 987−994.
(14) Kaur, S.; Sahoo, S.; Ajayan, P. M.; Kane, R. S. *Adv. Mater.* **2007**, *19*, 2984−2987.
(15) Ci, L.; Manikoth, S. M.; Li, X.; Vajtai, R.; Ajayan, P. M. *Adv. Mater.* **2007**, *19*, 3300−3303.
(16) Lim, X.; Foo, H. W. G.; Chia, G. H.; Sow, C. H. *ACS Nano* **2010**, *4*, 1067−1075.
(17) Liu, H.; Zhaia, J.; Jiang, L. *Soft Matter* **2006**, *2*, 811−821.
(18) Chakrapani, N.; Wei, B.; Carrillo, A.; Ajayan, P. M.; Kane, R. S. *Proc. Natl. Acad. Sci. U.S.A.* **2004**, *101*, 4009−4012.
(19) Cote, L. J.; Kim, F.; Huang, H. J. *J. Am. Chem. Soc.* **2009**, *131*, 1043−1049.
(20) Israelachvili, J. N. *Intermolecular and Surface Forces*, 2nd ed.; Academic Press: San Diego, 1992.
(21) Graf, D.; Molitor, F.; Ensslin, C.; Stampfer, C.; Jungen, A.; Hierold, C.; Wirtz, L. *Nano Lett.* **2007**, *7*, 238−242.
(22) Casiraghi, C.; Hartschuh, A.; Qian, S.; Piscance, S.; Georgi, C.; Fasoli, A.; Novoselov, K. S.; Basko, D. M.; Ferrari, A. C. *Nano Lett.* **2009**, *9*, 1433−1441.
(23) Kudin, K. N.; Ozbas, B.; Schniepp, H. C.; Prudhomme, R. K.; Aksay, I. A.; Car, R. *Nano Lett.* **2008**, *8*, 36−41.
(24) Conway, B. E. *Electrochemical Supercapacitors: Scientific Fundamentals and Technological Applications*; Plenum Publishers: New York, 1999.
(25) Du, C.; Yeh, J.; Pan, N. *Nanotechnology* **2005**, *16*, 350−353.
(26) Talapatra, S.; Kar, S.; Pal, S. K.; Vajtei, R.; Ci, L.; Victor, P.; Shaijumon, M. M.; Kaur, S.; Nalamasu, O.; Ajayan, P. M. *Nat. Nanotechnol.* **2006**, *1*, 112−116.
(27) Du, C.; Pan, N. *J. Power Sources* **2006**, *160*, 1487−1494.
(28) Chmiola, J.; Yushin, G.; Dash, R.; Gogotsi, Y. *J. Power Sources* **2006**, *158*, 765−772.
(29) Taberna, P. L.; Simon, P.; Fauvarque, J. F. *J. Electrochem. Soc.* **2003**, *150*, A292−A300.
(30) Lotya, M.; King, P. J.; Khan, U.; De, S.; Jonathan, N.; Coleman, J. N. *ACS Nano* **2010**, *4*, 3155−3162.
(31) Khan, U.; O'Neill, A.; Lotya, M.; De, S.; Coleman, J. N. *Small* **2010**, *6*, 864−871.

AM100343A